

Received March 23, 2021, accepted April 5, 2021, date of publication April 8, 2021, date of current version April 19, 2021.

Digital Object Identifier 10.1109/ACCESS.2021.3071829

# Multiple-Input Universal Filter and Quadrature Oscillator Using Multiple-Input Operational Transconductance Amplifiers

MONTREE KUMNGERN<sup>1</sup>, FABIAN KHATEB<sup>2,3</sup>, TOMASZ KULEJ<sup>4</sup>,  
AND COSTAS PSYCHALINOS<sup>5</sup>, (Senior Member, IEEE)

<sup>1</sup>Telecommunications Engineering Department, School of Engineering, King Mongkut's Institute of Technology Ladkrabang, Bangkok 10520, Thailand

<sup>2</sup>Department of Microelectronics, Brno University of Technology, 601 90 Brno, Czech Republic

<sup>3</sup>Faculty of Biomedical Engineering, Czech Technical University in Prague, 539 01 Kladno, Czech Republic

<sup>4</sup>Department of Electrical Engineering, Czestochowa University of Technology, 42-201 Czestochowa, Poland

<sup>5</sup>Electronics Laboratory, Physics Department, University of Patras, 265 04 Patras, Greece

Corresponding author: Montree Kumngern (montree.ku@kmitl.ac.th)

This work was supported by the School of Engineering, King Mongkut's Institute of Technology Ladkrabang under Grant 2563-02-01-027.

**ABSTRACT** This paper presents a new multiple-input single –output voltage-mode universal biquad filter based on multiple–input operational transconductance amplifiers (MI-OTA). This work demonstrates that the multiple-input OTA–based universal filter can provide more filtering responses and other benefits, compared to conventional OTA–based one. The filter provides electronic and orthogonal control of the natural frequency and the quality factor. Furthermore, a two-phase quadrature oscillator can be obtained by slightly modifying the proposed universal filter while the condition and frequency of oscillation can be controlled orthogonally and electronically. The performance of the proposed circuit is evaluated in Cadence environment using the TSMC 0.18  $\mu\text{m}$  CMOS technology. The voltage supply is 1.2 V and the power dissipation of the MI–OTA is 24  $\mu\text{W}$ . For 1% third intermodulation distortion (IMD3) the dynamic range of the band–pass filter is 78.6 dB. In addition, the proposed filter and oscillator are investigated through experiment tests using LM13700 commercially available OTA.

**INDEX TERMS** Universal filter, quadrature oscillator, operational transconductance amplifier, analog signal processing, voltage–mode circuit.

## I. INTRODUCTION

Analog filters are important signal processing blocks for electronic, communication and control systems applications. For instance, they are used to reject the out–of–band noise in electronic and control systems and to eliminate the carrier signal in communication systems [1]. Universal filters are the circuits that usually provide five standard filtering responses into single topology: low-pass (LP), high–pass (HP), band–pass (BP), band–stop (BS) and all–pass (AP) responses. The filters with orthogonal control of the natural frequency and the quality factor are the most desirable ones. Moreover, the voltage–mode filters with high input impedance and without inverting–type signal inputs are required to avoid additional buffers and inverting amplifiers.

The next important kind of electronic circuits are oscillators. They are used in electronic, telecommunication and

control systems to generate waveforms of different shapes, amplitudes and frequencies. Quadrature oscillators are the systems that usually generate two sinusoidal signals with 90° phase shift. They are often used in communication and measurement systems, such as quadrature mixers [1], vector generators, selective voltmeters [2], and many other. The circuits with orthogonal control of the condition of oscillation and the frequency of oscillations are the most desirable ones.

The operational transconductance amplifier (OTA) is the basic active block in OTA–C filter design [3]–[11]. However, more complex filters require relatively large number of OTAs, that increases the silicon area and power dissipation [12]. The multiple-input OTA (MI–OTA) appeared as an attractive alternative technique that reduces the number of single–input OTAs used in filter design [12]–[15]. The multiple–input OTA enables summing and subtracting signals at its inputs. It was claimed that the use of multiple-input OTAs could reduce the number of components, silicon area, and power dissipation by approximately the factor of  $k$ , where  $k$  is the

The associate editor coordinating the review of this manuscript and approving it for publication was Dušan Grujić.

number of inputs of the OTA [12]. As representative examples, one could provide the third- and seventh-order elliptic and low-pass filters described in [12] and [15]. Nevertheless, the MI-OTAs used in the aforementioned designs were based on parallel connections of differential stages to obtain the multiple-input blocks, resulting not only in increased number of transistors and chip area, but mainly in increased number of current branches, thus leading to a higher power dissipation and a more complex internal structure. A simple structure of MI-OTA, using one differential pair, can be achieved by employing the multiple-input floating-gate transistor (MIFG) [16]. Nevertheless, the MIFG transistor is based on charge conversation making it unpractical with modern CMOS technologies that suffer from gate leakage [17]. Furthermore, the MIFG transistor suffers from a residual charge on its gate, that results in higher voltage offset compared to conventional design.

This paper presents a new MI-OTA based universal filter, with more filtering responses and more versatility, and a quadrature oscillator. Unlike, the aforementioned MI-OTAs, the presented OTA use the multiple-input MOS transistor (MI-MOST) technique that allows simplifying its overall structure and decrease the power dissipation. It is worth noting that the first experimental results of MI-MOST were presented by Khateb et. al in [18]–[20]. Later, this technique has been used in several active blocks and applications [21]–[28].

This paper is organized as follows: Section 2 shows the multiple input OTA. Section 3 presents its applications in the active filter and oscillator circuit. Sections 4 and 5 present the non-ideal analysis and simulation results, respectively. The experimental results are shown in Section 6. Finally, the conclusion is given in Section 7.

## II. MULTIPLE-INPUT OTA

Fig. 1 (a) shows the circuit symbol of OTA. Its ideal characteristic can be described by

$$I_o = g_m (V_{1+} - V_{1-}) \quad (1)$$

where  $I_o$  is the output current,  $g_m$  is the transconductance gain,  $V_{1+}$  and  $V_{1-}$  denote, respectively, the voltage of the non-inverting and inverting input terminals.

The symbol of multiple-input OTA is shown in Fig. 1 (b). Its ideal characteristic can be described by

$$I_o = g_m \left( \sum_{i=1}^n V_{i+} - \sum_{i=1}^n V_{i-} \right) \quad (2)$$

where  $n$  is the number of required inputs.

In order to realize the multiple-input OTA, one could use  $n$  single-input OTAs with their outputs connected together, as shown in Fig. 1 (c). However, this realization results in increased chip area and power consumption that limits its usefulness in low-voltage and low-power applications. Alternative way to realize the multiple-input OTA is to use one OTA with  $n$  parallel-connected differential stages [12]–[14]. However, this method still suffers from increased chip area, and power consumption.

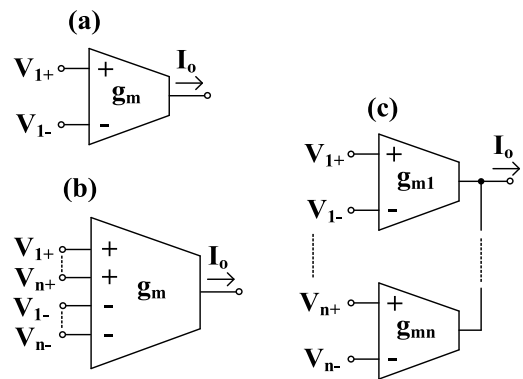


FIGURE 1. Circuit symbol of OTA, (a) single-ended OTA, (b) multiple-input OTA and (c) possible realization of multiple-input OTA.

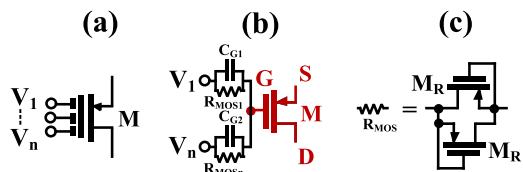


FIGURE 2. Multiple-input MOST: (a) symbol, (b) realization and, (c) realization of the large resistance value.

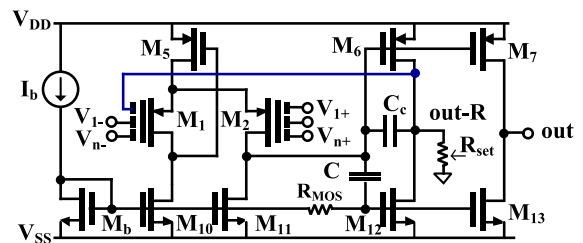
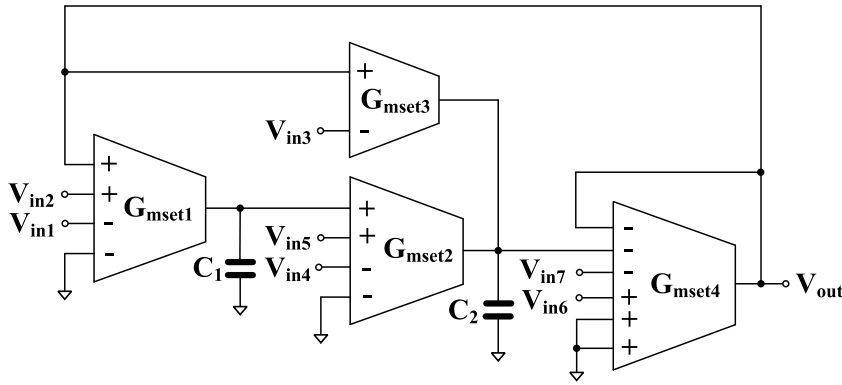


FIGURE 3. Multiple-input OTA.

The MI-OTA can be simply realized, using the MI-MOST [18]–[20]. The symbol of the MI-MOST with  $n$  inputs is depicted in Fig. 2 (a). The arbitrary number of inputs can be obtained by coupling the input terminals ( $V_1, \dots, V_n$ ) to the gate terminal (G) of the conventional MOST by  $n$  input capacitors ( $C_{G1}, \dots, C_{Gn}$ ). To ensure the DC signal path, the high resistances ( $R_{MOS1}, \dots, R_{MOSn}$ ), created by two MOSTs ( $M_R$ ) operating in cut-off region, are connected in parallel to each input capacitor, as shown in Fig. 2 (b) and (c). Due to the employment of the transistor  $M_R$  a high resistance value of the order of several  $G\Omega$  is simply obtained with minimum chip area. In this work, to realize the MI-OTA, a two-stage OTA with two outputs denoted as out-R and out is used, as shown in Fig. 3. The differential stage consists of one MI-MOST differential pair  $M_1, M_2$ , a flipped voltage follower  $M_5$ , and two current sources  $M_{10}, M_{11}$ . The second stage operates in so-called super class AB and consists of  $M_6$  and  $M_{12}$ . In this stage,  $R_{MOS}$  ensures the DC biasing of the gate of  $M_{12}$  while the capacitor  $C$  ensures the AC signal path to this gate [28].


**FIGURE 4.** Proposed universal biquad filter using MI-OTAs.

The capacitor  $C_C$  ensures the OTA stability. The negative feedback from the output terminal out-R to the input terminal of  $M_1$  ensures transferring of the differential input voltages to the output terminal with the voltage gain equal to unity. The output terminal out-R is connected to a linear adjustable resistor  $R_{set}$  that converts the output voltage to output current  $I_{Rset}$ . This current is mirrored by  $M_7$  and  $M_{13}$  to the output terminal out. Hence, the transconductance stage is obtained.

$$V_{out-R} = \left( \sum_{i=1}^n V_{i+} - \sum_{i=1}^n V_{i-} \right) \quad (3)$$

$$I_{out-R} = \frac{V_{out-R}}{R_{set}} = \frac{\left( \sum_{i=1}^n V_{i+} - \sum_{i=1}^n V_{i-} \right)}{R_{set}} \quad (4)$$

$$\begin{aligned} G_{meet} &= \frac{1}{R_{set}} = \frac{I_{out-R}}{\left( \sum_{i=1}^n V_{i+} - \sum_{i=1}^n V_{i-} \right)} \\ &= \frac{I_{out}}{\left( \sum_{i=1}^n V_{i+} - \sum_{i=1}^n V_{i-} \right)} \end{aligned} \quad (5)$$

It is worth mentioning that the proposed MI-OTA enjoys high linearity and increased input voltage range thanks to the negative feedback connection and the input capacitive divider, that attenuate the input signal. Furthermore, thanks to the flipped voltage follower, the minimum voltage supply is given by only one gate-source and one drain-source voltage ( $V_{DDmin} = V_{GS-M5} + V_{DS-M10}$ ).

### III. PROPOSED CIRCUITS

The proposed universal biquad filter using MI-OTAs is shown Fig. 4. It consists of four MI-OTAs and two grounded capacitors. If  $V_{in1}$ ,  $V_{in2}$ ,  $V_{in3}$ ,  $V_{in4}$ ,  $V_{in5}$ ,  $V_{in6}$  and  $V_{in7}$  are input voltages, the output voltage of the proposed filter can be expressed by

$$V_{out} = \frac{s^2 C_1 C_2 (V_{in6} - V_{in7}) + s C_1 G_{mset2} (V_{in4} - V_{in5}) + s C_1 G_{mset3} V_{in3} + G_{mset2} G_{mset1} (V_{in1} - V_{in2})}{s^2 C_1 C_2 + s C_1 G_{mset3} + G_{mset2} G_{mset1}} \quad (6)$$

where  $G_{mset1} = 1/R_{set1}$ ,  $G_{mset2} = 1/R_{set2}$ ,  $G_{mset3} = 1/R_{set3}$  and  $G_{mset4} = 1/R_{set4}$ .

From (6), five standard filtering responses and ten filtering functions can be obtained as

- (1) The non-inverting LP response:  $V_{in2} = V_{in3} = V_{in4} = V_{in5} = V_{in6} = V_{in7} = 0$  (grounded),  $V_{in1} = V_{in}$ .
- (2) The inverting LP response:  $V_{in1} = V_{in3} = V_{in4} = V_{in5} = V_{in6} = V_{in7} = 0$  (grounded),  $V_{in2} = V_{in}$ .
- (3) The non-inverting BP response:  $V_{in1} = V_{in2} = V_{in4} = V_{in5} = V_{in6} = V_{in7} = 0$  (grounded),  $V_{in3} = V_{in}$ .
- (4) The non-inverting BP response:  $V_{in1} = V_{in2} = V_{in3} = V_{in5} = V_{in6} = V_{in7} = 0$  (grounded),  $V_{in4} = V_{in}$ .
- (5) The inverting BP response:  $V_{in1} = V_{in2} = V_{in3} = V_{in4} = V_{in6} = V_{in7} = 0$  (grounded),  $V_{in5} = V_{in}$ .
- (6) The non-inverting HP response:  $V_{in1} = V_{in2} = V_{in3} = V_{in4} = V_{in5} = V_{in7} = 0$  (grounded),  $V_{in6} = V_{in}$ .
- (7) The inverting HP response:  $V_{in1} = V_{in2} = V_{in3} = V_{in4} = V_{in5} = V_{in6} = 0$  (grounded),  $V_{in7} = V_{in}$ .
- (8) The non-inverting BS response:  $V_{in2} = V_{in3} = V_{in4} = V_{in5} = V_{in7} = 0$  (grounded),  $V_{in1} = V_{in6} = V_{in}$ .
- (9) The inverting BS response:  $V_{in1} = V_{in3} = V_{in4} = V_{in5} = V_{in6} = 0$  (grounded),  $V_{in2} = V_{in7} = V_{in}$ .
- (10) The non-inverting AP response:  $V_{in2} = V_{in3} = V_{in4} = V_{in7} = 0$  (grounded),  $V_{in1} = V_{in5} = V_{in6} = V_{in}$ .
- (11) The inverting AP response:  $V_{in1} = V_{in3} = V_{in5} = V_{in6} = 0$  (grounded),  $V_{in2} = V_{in4} = V_{in7} = V_{in}$ .

The parameters  $\omega_o$  and  $Q$  of all filtering responses can be expressed as

$$\omega_o = \sqrt{\frac{G_{mset2} G_{mset1}}{C_1 C_2}} \quad (7)$$

$$Q = \frac{1}{G_{mset3}} \sqrt{\frac{C_2 G_{mset2} G_{mset1}}{C_1}} \quad (8)$$

Letting  $G_{mset1} = G_{mset2} = G_{mset}$ , (7) and (8) can be rewritten as

$$\omega_o = \frac{G_{mset}}{\sqrt{C_1 C_2}} \quad (9)$$

$$Q = \frac{G_{mset}}{G_{mset3}} \sqrt{\frac{C_2}{C_1}} \quad (10)$$

From (9) and (10), the parameter  $\omega_o$  for all filtering responses can be controlled electronically through  $G_{mset}$  ( $G_{mset} = G_{mset1} = G_{mset2}$ ) with constant  $C_1 = C_2$  while the parameter  $Q$  can be controlled orthogonally through  $G_{mset3}$  with

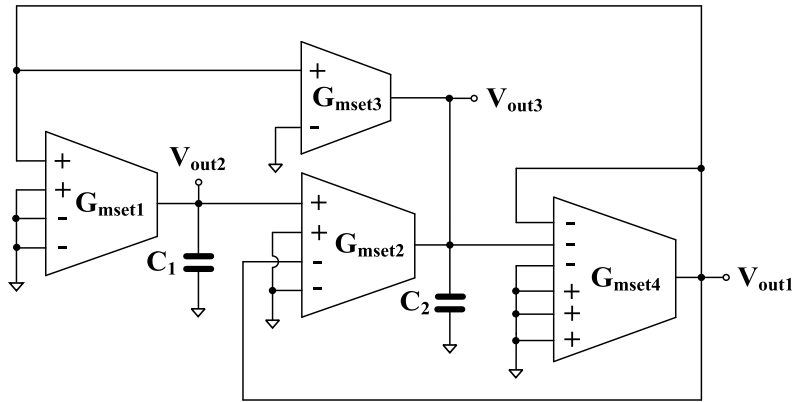


FIGURE 5. Quadrature oscillator developed from the universal filter.

constant  $G_{mset}$  ( $G_{mset} = G_{mset1} = G_{mset2}$ ), and  $C_1 = C_2$ . In case of non-inverting and inverting all-pass responses, a condition  $G_{mset2} = G_{mset3}$  is required.

The universal biquad filter in Fig. 4 can be transformed to a quadrature oscillator as shown in Fig. 5. To obtain orthogonal control of the condition of oscillation and the frequency of oscillations, the non-inverting band-pass response  $V_{in4}$  could be used to create a positive feedback loop, with inputs  $V_{in1}$ ,  $V_{in2}$ ,  $V_{in3}$ ,  $V_{in5}$ ,  $V_{in6}$  and  $V_{in7}$  connected to ground. The characteristic equation of the quadrature oscillator can be expressed by

$$s^2 C_1 C_2 + s C_1 (G_{mset3} - G_{mset2}) + G_{mset1} G_{mset2} = 0 \quad (11)$$

The condition of oscillations (CO) and the frequency of oscillations (FO) can be expressed, respectively, by

$$G_{mset2} = G_{mset3} \quad (12)$$

$$\omega_o = \sqrt{\frac{G_{mset1} G_{mset2}}{C_1 C_2}} \quad (13)$$

From (12) and (13), it is evident that CO can be controlled electronically by  $G_{mset3}$ , while FO can be varied orthogonally by  $G_{mset1}$  with  $C_1 = C_2$  constant. Thus, the quadrature oscillator can be orthogonally controlled. It should be noted that the quadrature oscillator in Fig. 5 provides three output terminals  $V_{out1}$ ,  $V_{out2}$  and  $V_{out3}$ . The additional outputs still provide sinusoidal signals, with  $90^\circ$  phase shift, and the relationships between output signals can be expressed as:

$$\frac{V_{out2}}{V_{out1}} = \frac{G_{mset1}}{s C_1} \quad (14)$$

$$\frac{V_{out3}}{V_{out2}} = \frac{G_{mset2}}{s C_2} \quad (15)$$

With  $s = j\omega_o$ , eqns. (14) and (15) can be rewritten respectively, as  $V_{out1} = j(\omega_o C_1 / G_{mset1}) V_{out2}$  and  $V_{out2} = j(\omega_o C_2 / G_{mset2}) V_{out3}$  which indicates that  $V_{out1}$  with  $V_{out2}$ , and  $V_{out2}$  with  $V_{out3}$  remain in quadrature.

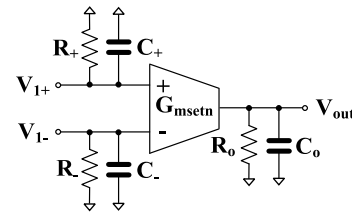


FIGURE 6. Modeling the non-idealities in the OTA.

#### IV. NON-IDEAL ANALYSIS

Considering non-idealities of OTA, the transconductance gain  $G_{msetnj}$  can be expressed as [29]

$$G_{msetnj}(s) = \frac{G_{msetj} \omega_{gj}}{s + \omega_{gj}} \quad (16)$$

where  $\omega_{gj}$  denote the pole frequency of  $OTA_j$  ( $j = 1, 2, \dots, n$ ). In the frequency range of a few MHz,  $G_{msetnj}$  can be modified as

$$G_{msetnj}(s) \cong G_{msetj} (1 - \mu_j s) \quad (17)$$

where  $\mu_j = 1/\omega_{gj}$ . The pole frequency  $\omega_{gj}$ , results from the parasitic input and output resistances ( $R_+$ ,  $R_-$ ,  $R_o$ ) and the input and output capacitances ( $C_+$ ,  $C_-$ ,  $C_o$ ), as shown in Fig. 6. The high-resistance and small-capacitance values will result in high value of  $\omega_{gj}$  and small value of  $\mu_j$ .

Using (17), the denominator of the transfer function of the universal filter can be expressed as

$$s^2 C_1 C_2 \left( 1 - \frac{C_1 G_{mset3} \mu_3 - G_{mset1} G_{mset2} \mu_1 \mu_2}{C_1 C_2} \right) + s C_1 G_{mset3} \left( 1 - \frac{G_{mset1} G_{mset2} \mu_1 + G_{mset1} G_{mset2} \mu_2}{C_1 G_{mset3}} \right) + G_{mset2} G_{mset1} \quad (18)$$

It can be made negligible by satisfying the following, condition:

$$\frac{C_1 G_{mset3} \mu_3 - G_{mset1} G_{mset2} \mu_1 \mu_2}{C_1 C_2} \ll 1 \quad (19)$$

$$\frac{G_{mset1} G_{mset2} \mu_1 + G_{mset1} G_{mset2} \mu_2}{C_1 G_{mset3}} \ll 1 \quad (20)$$

**TABLE 1.** Parameters of the components of MI-OTA in Fig. 2.

Transistor	W/L (μm/ μm)
M <sub>1</sub> , M <sub>2</sub> , M <sub>5</sub>	9×9/0.3
M <sub>b</sub> , M <sub>10</sub> , M <sub>11</sub>	12/3
M <sub>12</sub> , M <sub>13</sub>	2×12/3
M <sub>6</sub> , M <sub>7</sub>	2×25/2
M <sub>R</sub>	4/5
C <sub>G</sub> =0.5 pF, C <sub>c</sub> = C = 2.6pF	

The various passive and active sensitivities of the parameters ω<sub>o</sub> and Q of the universal filter can be expressed as

$$S_{G_{mset1}}^{\omega_o} = S_{G_{mset2}}^{\omega_o} = -S_{C_1}^{\omega_o} = -S_{C_2}^{\omega_o} = \frac{1}{2} \quad (21)$$

$$S_{G_{mset1}}^Q = S_{G_{mset2}}^Q = S_{C_2}^Q = -S_{C_1}^Q = \frac{1}{2} \quad (22)$$

$$S_{G_{mset3}}^Q = -1 \quad (23)$$

Thus, all the incremental parametric sensitivities for parameters ω<sub>o</sub> and Q are below 1.

Using (17), the characteristic equation of a quadrature oscillator can be written as

$$s^2 C_1 C_2 \left( 1 - \frac{C_1 G_{mset3} \mu_3 - C_1 G_{mset2} \mu_2 - G_{mset1} G_{mset2} \mu_1 \mu_2}{C_1 C_2} \right) + s C_1 (G_{mset3} - G_{mset2}) \times \left( 1 - \frac{G_{mset1} G_{mset2} \mu_2 - G_{mset1} G_{mset2} \mu_1}{C_1 (G_{mset3} - G_{mset2})} \right) + G_{mset1} G_{mset2} = 0 \quad (24)$$

It can be made negligible by satisfying the following condition:

$$\frac{C_1 G_{mset3} \mu_3 - C_1 G_{mset2} \mu_2 - G_{mset1} G_{mset2} \mu_1 \mu_2}{C_1 C_2} \ll 1 \quad (25)$$

$$\frac{G_{mset1} G_{mset2} \mu_2 - G_{mset1} G_{mset2} \mu_1}{C_1 (G_{mset3} - G_{mset2})} \ll 1 \quad (26)$$

**V. SIMULATION RESULTS**

The circuit was designed to work with 1.2 V supply, with 5 μA bias current and 24 μW power consumption. The Cadence environment has been used to design and simulate the circuit using a 0.18μm CMOS technology from TSMC. The parameters of the components are shown in Table. 1.

For the filter design the capacitor C<sub>1</sub> = C<sub>2</sub> = 10 nF and R<sub>set1</sub> = R<sub>set2</sub> = R<sub>set3</sub> = R<sub>set4</sub> = 15 kΩ were selected for natural frequency of 1 kHz. These R<sub>set</sub> resistors can be integrated on chip using a high resistance poly resistor while these 10 nF capacitors should be off-chip capacitors.

The simulated magnitude frequency responses of the universal filter showing the non-inverting LP, HP, BP, and BS responses are shown in Fig. 7. The simulated natural frequency is 1.03 kHz. The magnitude frequency response and the phase characteristic of the non-inverting AP filter are shown in Fig. 8. The total power consumption of the filter is 96 μW. Fig. 9 shows the tuning capability of the Q factor

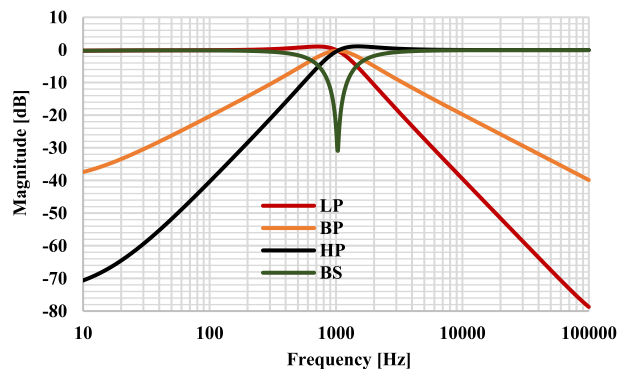


**FIGURE 7.** The simulated magnitude frequency responses of the universal filter.

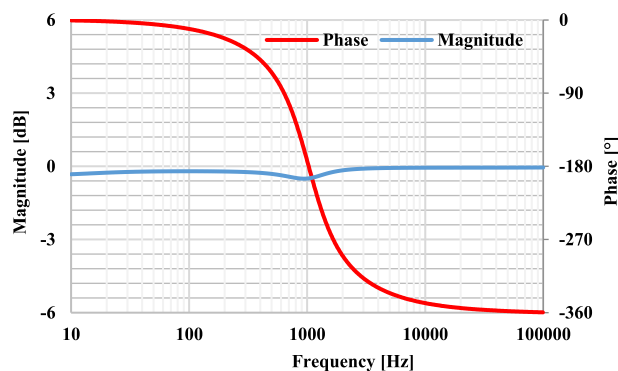


**FIGURE 8.** The simulated magnitude frequency response and phase characteristic of the AP filter.

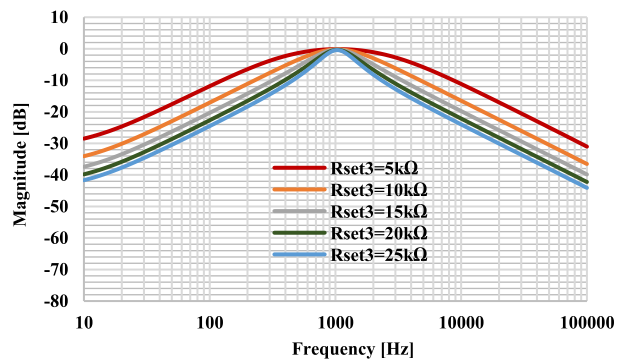


**FIGURE 9.** The simulated tuning capability of the BP filter.

for the BP filter by tuning R<sub>set3</sub> = 5kΩ, 10kΩ, 15kΩ, 20kΩ and 25kΩ, while R<sub>set1</sub> = R<sub>set2</sub> = R<sub>set4</sub> = 15kΩ.

A sine wave with different amplitudes (0.05V, 0.1V, 0.15V, 0.2V, 0.25V) and 1 kHz frequency was applied to the input of the BP filter. The output signals are shown in Fig. 10. The total harmonic distortion (THD) is less than 1.67 % for input amplitude of 0.3V as shown in Fig. 11. This confirms the high linearity of the filter with low THD.

To determine the third-order distortion products produced by the circuit nonlinearity, two tones that are close in frequency are applied to the input of the BP filter. The first

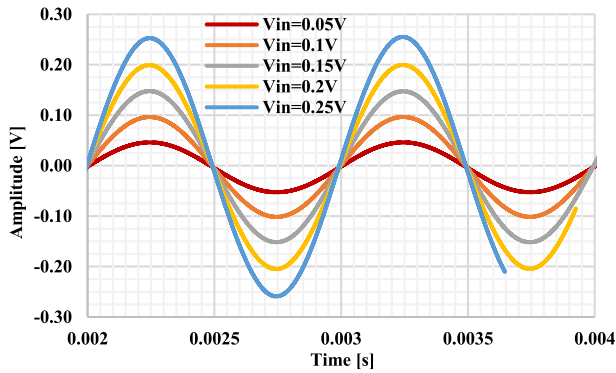


**FIGURE 10.** The simulated transient analysis of the BP filter with different amplitude of input signal at 1kHz.

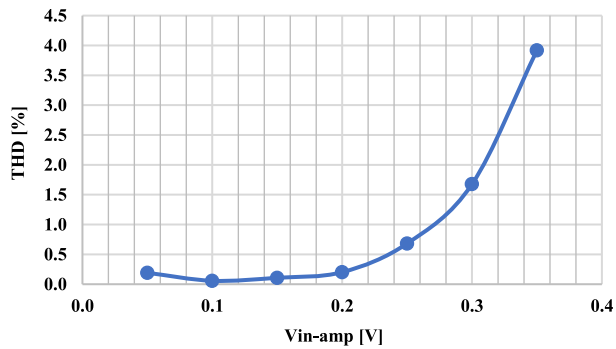


**FIGURE 11.** The simulated transient analysis of the BP filter with different amplitude of input signal at 1kHz.

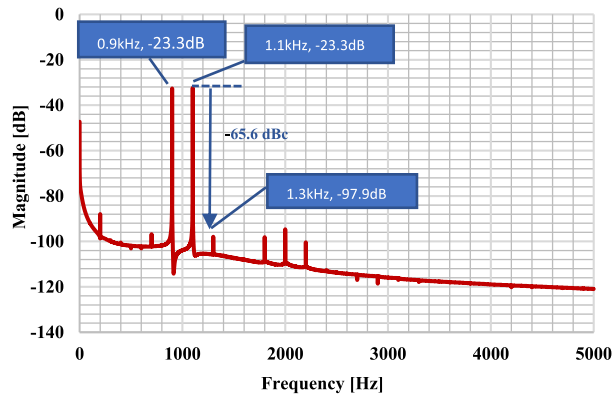


**FIGURE 12.** The simulated spectrum of the output signal of the BP filter.

tone is a sine wave with amplitude of 25mV@ 0.9kHz and the second one with 25mV@ 1.1kHz. The spectrum of the output signal is depicted in Fig. 12. The third intermodulation distortion (IMD3) is only -65.6 dBc. The relation between the IMD3 and the peak-to-peak value of the input signal is shown in Fig. 13. The IMD3 is around -33.7 dB for 350mV<sub>pp</sub>. The equivalent output noise of the BPF is shown in Fig. 14. The RMS output noise of the BP filter integrated in the band pass from 432Hz–2.523kHz was 12μV that results in 78.6dB dynamic range for 1% IMD3.

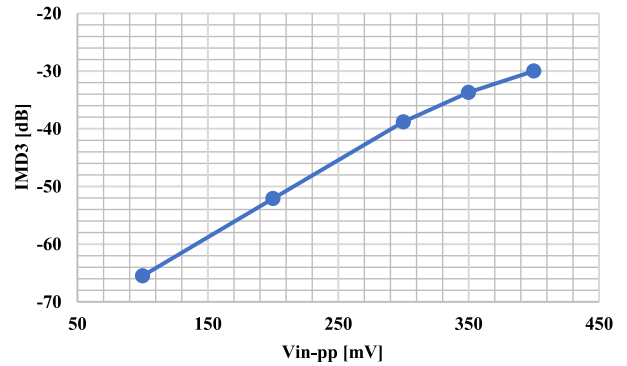


**FIGURE 13.** The simulated IMD3 versus the input signal ( $V_{in-pp}$ ) for the BP filter.

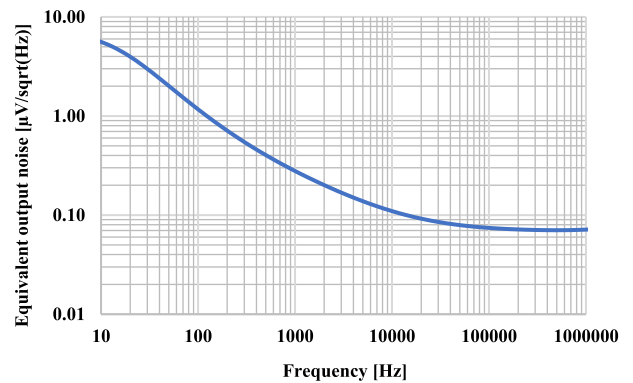


**FIGURE 14.** The simulated equivalent output noise of the BPF.

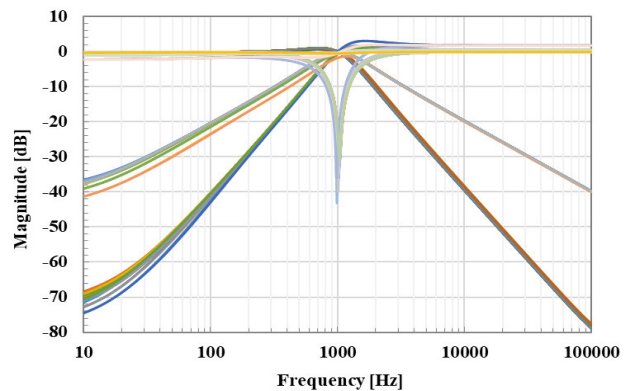


**FIGURE 15.** The simulated magnitude frequency responses of the universal filter with PVT corners.

To confirm the robustness of the design under process, voltage, temperature (PVT) corners, the MOS transistor (slow–slow, slow –fast, fast–slow, fast–fast), MIM-capacitor (slow–slow, fast–fast), voltage supply ( $V_{DD} \pm 10\%$ ), and temperature ( $-10^{\circ}\text{C} - 60^{\circ}\text{C}$ ) corners were selected. Fig. 15 shows the magnitude frequency responses for the circuits of Figs. 7 and 8 with PVT corners and confirm the robustness of the design.

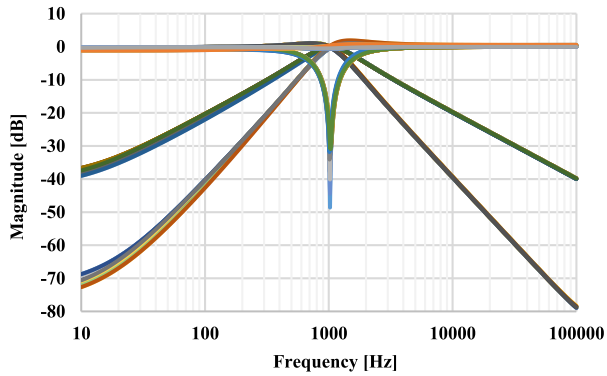


FIGURE 16. The simulated magnitude frequency responses of the universal filter with 200 runs MC analysis.

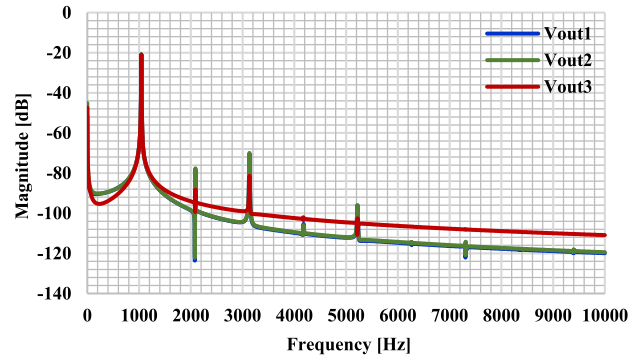


FIGURE 19. The simulated spectrums of the output signals.

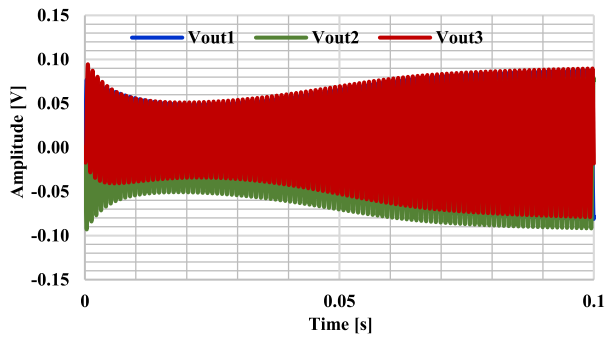


FIGURE 17. The simulated growing oscillations of the quadrature oscillator output voltages.

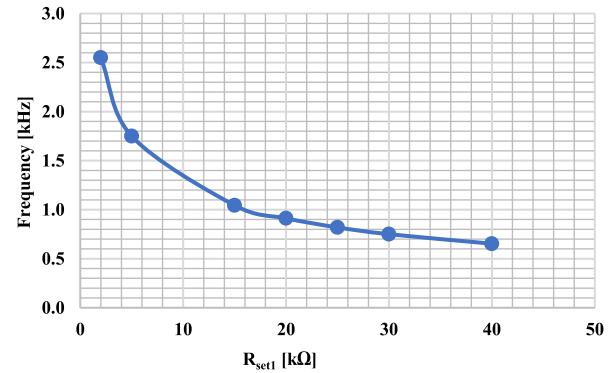


FIGURE 20. The simulated oscillator frequency versus  $R_{set1}$ .

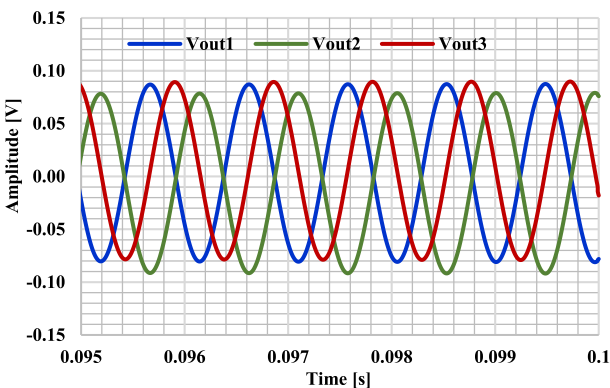


FIGURE 18. The simulated steady-state output waveforms of the oscillation.

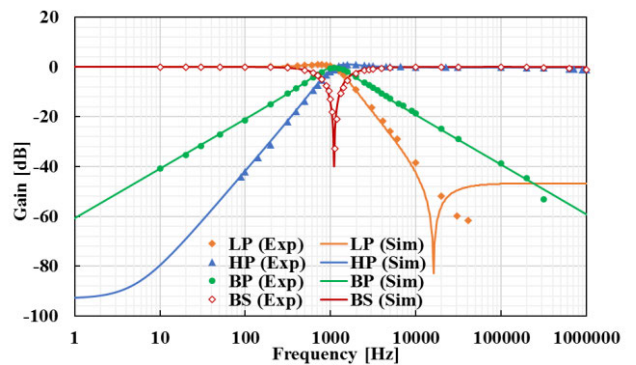


FIGURE 21. The measured and simulated frequency magnitude responses of the LP, BP, HP and BS filters.

The low sensitivity of the design to process and mismatch variation was also proved by Monte Carlo (MC) analysis with 200 runs as shown in Fig. 16.

The quadrature oscillator was also simulated with  $C_1 = C_2 = 10\text{nF}$ ,  $R_{set1} = R_{set2} = R_{set4} = 15\text{k}\Omega$ . To start the oscillation the  $R_{set3}$  was selected to  $16\text{k}\Omega$ . The simulated oscillation frequency was  $1.04\text{kHz}$ . Fig. 17 shows the growing oscillations of the oscillator output voltage  $V_{out1}$ ,  $V_{out2}$  and  $V_{out3}$  while Fig. 18 shows the steady-state waveforms. The spectrum of the output signals was shown in Fig. 19, the THD of the output signals is  $0.33\%$ ,  $0.35\%$  and  $0.1\%$  for  $V_{out1}$ ,  $V_{out2}$ ,  $V_{out3}$ , respectively.

Fig. 20 shows the frequency versus  $R_{set1}$ . For all simulated frequencies, the THD was less than  $0.4\%$ .

## VI. EXPERIMENTAL RESULTS

The proposed universal filter was also tested experimentally. The prototype circuit was realized using commercially available integrated circuits LM13700N [30]. Note, that the macro-model of the LM13700N has been also used, hence the simulation results based on macro-model and the measured results can be compared. The multiple input OTA was realized by a parallel connection of OTAs (LM13700N) as shown in Fig. 1 (c).

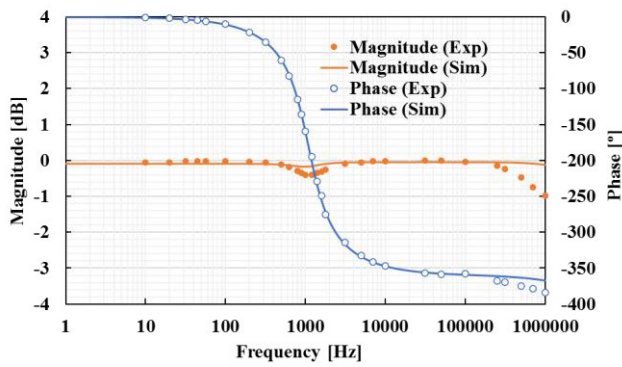


FIGURE 22. The measured and simulated frequency magnitude and phase responses of the AP filter.

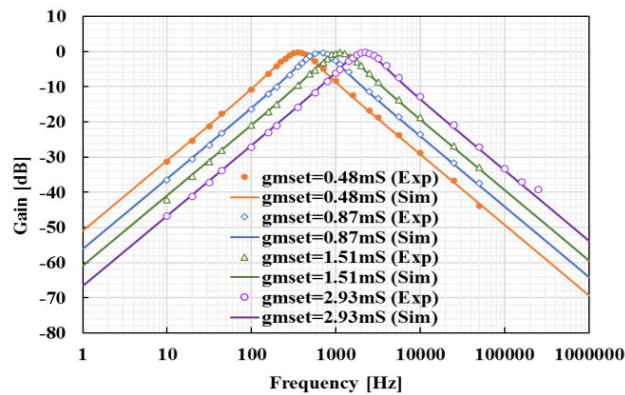


FIGURE 23. The measured and simulated magnitude responses of the BP filter with different parameter  $\omega_0$ .

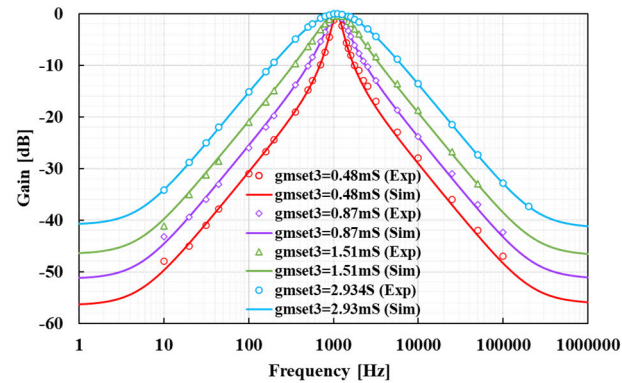


FIGURE 24. The measured and simulated magnitude responses of the BP filter with different parameter  $Q$ .

The supply voltages were  $V_{DD} = -V_{SS} = 5$  V and the capacitances  $C_1$  and  $C_2$  were of 220 nF. The sinusoidal input signal and the output waveforms were measured using Agilent Technologies DSOX 1102G oscilloscope. The transconductances  $g_{mset1} = g_{mset2} = g_{mset3} = g_{mset4} = 1.512$  mS were designed to obtain the filter with the natural frequency  $f_0 \cong 1.09$  kHz and the quality factor  $Q \cong 1$ . Fig. 21 shows the measured and simulated magnitude responses of the non-inverting LP, HP, BP and BS filter with natural frequency  $f_0 = 1.09$  kHz. Fig. 22 shows magnitude and phase responses

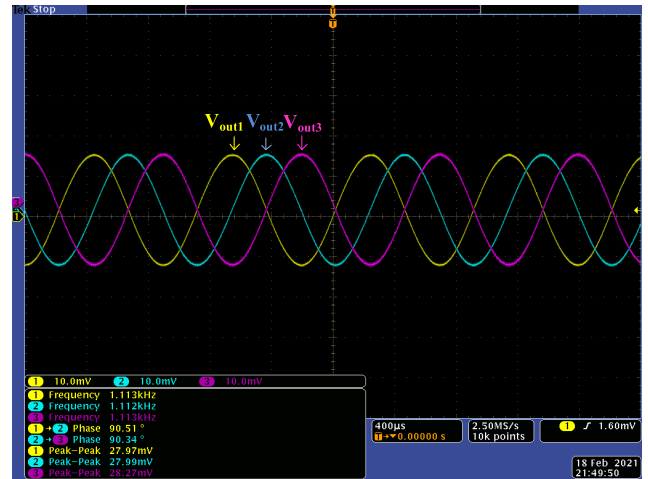
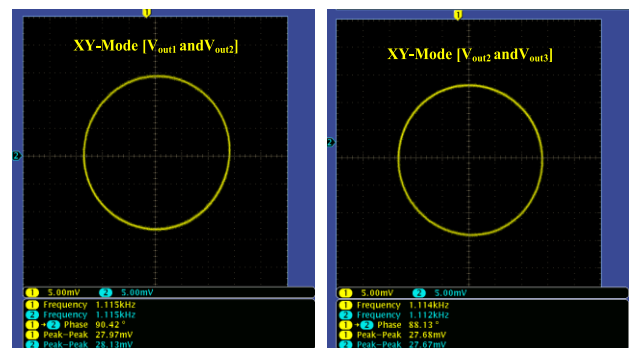


FIGURE 25. The experimental result of the quadrature outputs  $V_{out1}$ ,  $V_{out2}$ ,  $V_{out3}$ .



(a) (b)

FIGURE 26. Lissajous pattern: (a)  $V_{out1}$  and  $V_{out2}$  outputs, (b)  $V_{out2}$  and  $V_{out3}$  outputs.

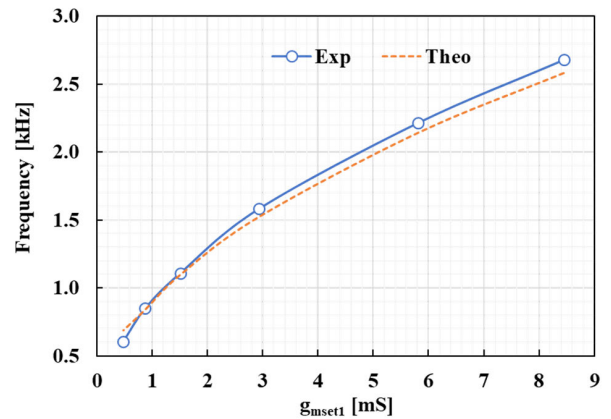


FIGURE 27. The measured and experimental frequency of oscillations versus  $g_{mset1}$ .

of the AP filter. Fig. 23 shows magnitude responses of the BP filters for different values of the transconductance  $g_{mset}$  ( $g_{mset} = g_{mset1} = g_{mset2} = g_{mset3}$ ) equal to 0.481 mS, 0.873 mS, 1.512 mS and 2.934 mS.

Fig. 24 shows the magnitude responses of the BP filters for  $g_{mset3}$  equal to 0.481 mS, 0.873 mS, 1.512 mS and 2.934 mS.

TABLE 2. Properties comparison of this work with those of OTA-based universal filters.

Factor	[6]	[7]	[8]	[9]	[10]	[11]	Proposed
Number of active devices	3-OTA/1-1 NV	5-OTA	5-OTA	5-OTA	5-OTA	1-DO-OTA, 3-OTA	4-MI-OTA
Realization	CMOS structure	commercial IC	commercial IC	commercial IC	CMOS structure	commercial IC	CMOS structure & commercial IC
Number capacitors	2-C	2-C	2-C	2-C	2-C	2-C	2-C
Total capacitance (nF)	0.002	4	4.4	2	0.02736	4.4	20
Type of filter	MISO	MISO	MIMO	MIMO	MISO	MIMO	MISO
Operation mode	MM	VM	VM	VM	MM	VM	VM
Number of offered responses	20 (5-VM)	5	13	24	20 (5-VM)	9	11
Offer inverting and non-inverting of five standard responses	Yes	No	No	No	No	No	Yes
All grounded capacitors	Yes	Yes	Yes	Yes	Yes	Yes	Yes
Unnecessary inverting input conditions	Yes	Yes	Yes	Yes	Yes	Yes	Yes
High input impedances	Yes	Yes	Yes	Yes	Yes	Yes	Yes
Orthogonal control of $\omega_o$ and $Q$	Yes	Yes	Yes	Yes	Yes	Yes	Yes
Offer modified into oscillator	No	Yes	Yes	Yes	No	Yes	Yes
Number phases of quadrature output	-	2	2	2	2	2	3
Simulated power supply (V)	$\pm 0.5$	$\pm 15$	$\pm 15$	$\pm 15$	$\pm 0.9$	$\pm 15$	1.2
Natural frequency (kHz)	2500	238.73	217	159.16	3390	144.7	1
Simulated power dissipation (mW)	0.035	-	860	861	-	920	0.096
Total harmonic distortion (%)	2@60mV <sub>pp</sub>	1.99@65mV <sub>pp</sub>	1.93@200mV <sub>pp</sub>	2@100mV <sub>pp</sub>	-	3.83 @170mV <sub>pp</sub>	1.67@600mV <sub>pp</sub>
IMD3 (dBc)	-	-33@40mV <sub>pp</sub>	-34@120mV <sub>pp</sub>	-34@60mV <sub>pp</sub>	-	-48.67@63mV <sub>pp</sub>	-52.1@200mV <sub>pp</sub>
Dynamic range (dB)	-	-	-	-	-	-	78.6
Verification of result	Sim	Sim/Exp	Sim/Exp	Sim/Exp	Sim	Sim/Exp	Sim/Exp

Note: MISO = multiple-input single output, MIMO = multiple-input multiple-output, INV = inverter, MM = mixed-mode, VM = voltage-mode, Sim = simulation, Exp = experimental, DO-OTA = dual-output OTA.

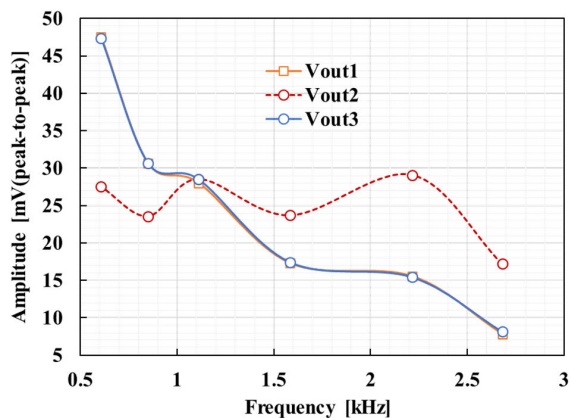


FIGURE 28. The measured output amplitudes versus frequency of oscillations.

The value of  $g_{mset3}$  was varied to obtain different values of the parameter  $Q$ , while the input signal was applied to  $V_{in3}$ , with  $g_{mset1} = g_{mset2} = 1.512$  mS.

The proposed quadrature oscillator was experimentally tested as well. The capacitances  $C_1$  and  $C_2$  were 220nF. The measured output waveforms were taken using Tektronix MSO 4034 mixed signal oscilloscope. Fig. 25 shows the measured output wave forms of  $V_{out1}$ ,  $V_{out2}$  and  $V_{out3}$  for  $g_{mset1} = g_{mset2} = g_{mset4} = 1.512$ mS and variable  $g_{mset3}$ , for controlling the condition of oscillation. The circuit generates the output waveform with frequency of 1.11 kHz, while the theoretical value was 1.09 kHz. The amplitudes were nearly equal in this case. The quadrature output waveform

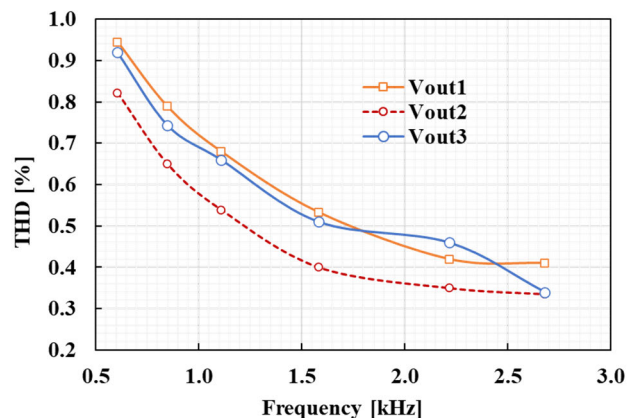
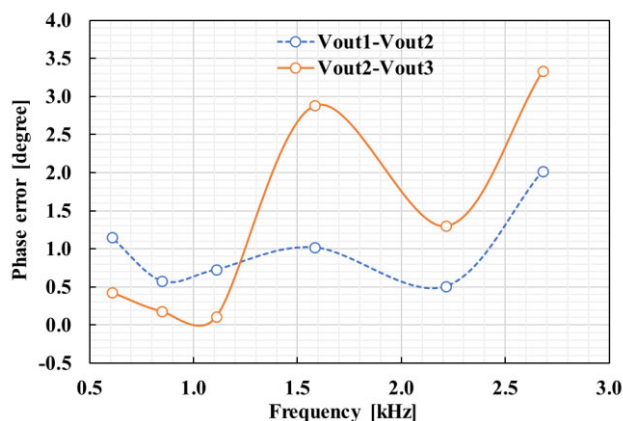


FIGURE 29. The measured THD of oscillations versus frequency.

in Fig. 25 was verified through the XY mode to show the quadrature relationship. The quadrature relationships between  $V_{out1}$  and  $V_{out2}$  and between  $V_{out2}$  and  $V_{out3}$  were shown in Fig. 26, (a) and (b), respectively. The measured frequency of oscillations as a function of  $g_{mset1}$  is shown in Fig. 27. The achieved results agree well with (13). The frequency of oscillations was 0.607 kHz, 0.849 kHz, 1.11 kHz, 1.58 kHz, 2.21 kHz and 2.68 kHz for  $g_{mset1}$  equal to 0.481 mS, 0.873 mS, 1.512 mS, 2.934 mS, 5.81 mS and 8.45 mS, respectively. The plot showing the output amplitude versus frequency of oscillations is shown in Fig. 28. The THD of the output signals  $V_{out1}$ ,  $V_{out2}$  and  $V_{out3}$  is shown in Fig. 29. The phase error between  $V_{out1}$  and  $V_{out2}$ , and between  $V_{out2}$  and  $V_{out3}$ , referred to  $90^\circ$ , is shown in Fig. 30.



**FIGURE 30.** The measured phase error as a function of frequency of oscillations.

Table. 2. compares the proposed circuit with most recent published works [6]–[11]. While the works in [7]–[9], [11] use only commercially available integrated circuit without CMOS structure, the works in [6], [10] use only a conventional CMOS OTA structure (i.e. well known OTA with one input).

Compared with [6], the proposed filter can be easily transformed into a quadrature oscillator. Although using the topology in [6] one can obtain five standard filtering responses, they are achievable only with the use of different modes of operation (voltage–mode, current–mode, transresistance–mode, transconductance–mode). Compared with [8]–[10], the proposed filter provides full non-inverting and inverting realization of five standard filtering responses and offers a three–phase quadrature oscillator. Furthermore, thanks to innovative and simple CMOS structure, the proposed filter offers improved linearity, lowest THD and IMD3, wide dynamic range and low power consumption and less amounts of active elements when it is realized using MI–OTAs. Finally, it is worth to mention that due to absence of MI-OTA fabrication the commercially available integrated circuit LM13700N is used only to confirm the functionality and benefits of the multiple-input technique on these new presented applications.

## VII. CONCLUSION

In this paper, a new voltage-mode universal biquad filter employing four MI–OTAs and two grounded capacitors is proposed. It offers eleven filtering responses into single topology which can be possible using the MI–OTA–based circuit. The filter also provides orthogonal control of the natural frequency and the quality factor. By slightly modifying the proposed universal filter, a two–phase quadrature oscillator with orthogonal control of the condition and frequency of oscillation can be obtained. The performance of the proposed filter and oscillator circuit were evaluated in Cadence environment using the TSMC 0.18  $\mu\text{m}$  CMOS technology and investigated by experiment tests using LM13600 discrete

component integrated circuit as OTAs. The simulation results were in consistent with the experimental ones.

## REFERENCES

- [1] S. Haykin, M. Moher, *An Introduction to Analog and Digital Communications*. New York, NY, USA: Wiley, 2007.
- [2] J.-W. Horng, C.-L. Hou, C.-M. Chang, W.-Y. Chung, H.-W. Tang, and Y.-H. Wen, “Quadrature oscillators using CCIIIs,” *Int. J. Electron.*, vol. 92, no. 1, pp. 21–31, Jan. 2005.
- [3] Y. Sun and J. K. Fidler, “Structure generation of current-mode two integrator loop dual output-OTA grounded capacitor filters,” *IEEE Trans. Circuits Syst. II. Analog Digit. Signal Process.*, vol. 43, no. 9, pp. 659–663, Sep. 1996.
- [4] C. Psychalinos, C. Kasimis, and F. Khateb, “Multiple-input single-output universal biquad filter using single output operational transconductance amplifiers,” *AEU-Int. J. Electron. Commun.*, vol. 93, pp. 360–367, Sep. 2018.
- [5] M. Kumngern, P. Suksaibul, and F. Khateb, “Four-input one-output voltage-mode universal filter using simple OTAs,” *J. Circuits, Syst., Comput.*, vol. 28, May 2019, Art. no. 1950078.
- [6] M. Parvizi, “Design of a new low power MISO multi-mode universal biquad OTA-C filter,” *Int. J. Electron.*, vol. 106, pp. 440–454, Mar. 2019.
- [7] S.-F. Wang, H.-P. Chen, Y. Ku, and C.-M. Yang, “A voltage-mode universal filter using five single-ended OTAs with two grounded capacitors and a quadrature oscillator using the voltage-mode universal filter,” *Optik*, vol. 192, Sep. 2019, Art. no. 162950.
- [8] S.-F. Wang, H.-P. Chen, Y. Ku, and C.-M. Yang, “Independently tunable voltage-mode OTA-C biquadratic filter with five inputs and three outputs and its fully-uncoupled quadrature sinusoidal oscillator application,” *AEU-Int. J. Electron. Commun.*, vol. 110, Oct. 2019, Art. no. 152822.
- [9] S.-F. Wang, H.-P. Chen, Y. Ku, and Y.-C. Lin, “Versatile tunable voltage-mode biquadratic filter and its application in quadrature oscillator,” *Sensors*, vol. 19, no. 10, p. 2349, May 2019.
- [10] D. R. Bhaskar, A. Raj, and P. Kumar, “Mixed-mode universal biquad filter using OTAs,” *J. Circuits, Syst., Comput.*, vol. 29, Aug. 2020, Art. no. 2050162.
- [11] S.-F. Wang, H.-P. Chen, Y. Ku, and C.-L. Lee, “Versatile voltage-mode biquadratic filter and quadrature oscillator using four OTAs and two grounded capacitors,” *Electronics*, vol. 9, no. 9, p. 1493, Sep. 2020.
- [12] A. Wyszynski and R. Schaumann, “Using multiple-input transconductors to reduce number of components in OTA-C filter design,” *Electron. Lett.*, vol. 28, pp. 217–220, Jan. 1992.
- [13] D. H. Chiang and R. Schaumann, “A CMOS fully-balanced continuous-time IFLF filter design for read/write channels,” in *Proc. IEEE Int. Symp. Circuits Syst. Circuits Syst. (ISCAS)*, Atlanta, GA, USA, Oct. 1996, pp. 167–170, doi: 10.1109/ISCAS.1996.539835.
- [14] V. Gopinathan, Y. P. Tsvividis, K.-S. Tan, and R. K. Hester, “Design considerations for high-frequency continuous-time filters and implementation of an antialiasing filter for digital video,” *IEEE J. Solid-State Circuits*, vol. 25, no. 6, pp. 1368–1378, Dec. 1990.
- [15] J. Glinianowicz, J. Jakusz, S. Szczepanski, and Y. Sun, “High-frequency two-input CMOS OTA for continuous-time filter applications,” *IEE Proc. - Circuits, Devices Syst.*, vol. 147, no. 1, pp. 13–18, Feb. 2000, doi: 10.1049/ip-cds:20000317.
- [16] A. J. Lopez-Martin, J. Ramirez-Angulo, R. G. Carvajal, and L. Acosta, “CMOS transconductors with continuous tuning using FGMS balanced output current scaling,” *IEEE J. Solid-State Circuits*, vol. 43, no. 5, pp. 1313–1323, May 2008.
- [17] H. D. Rico-Aniles, J. Ramirez-Angulo, A. J. Lopez-Martin, and R. G. Carvajal, “360 nW gate-driven ultra-low voltage CMOS linear transconductor with 1 MHz bandwidth and wide input range,” *IEEE Trans. Circuits Syst. II, Exp. Briefs*, vol. 67, no. 11, pp. 2332–2336, Nov. 2020.
- [18] F. Khateb, T. Kulej, M. Kumngern, and C. Psychalinos, “Multiple-input bulk-driven MOS transistor for low-voltage low-frequency applications,” *Circuits, Syst., Signal Process.*, vol. 38, no. 6, pp. 2829–2845, Jun. 2019.
- [19] F. Khateb, T. Kulej, H. Veldandi, and W. Jaikla, “Multiple-input bulk-driven quasi-floating-gate MOS transistor for low-voltage low-power integrated circuits,” *AEU-Int. J. Electron. Commun.*, vol. 100, pp. 32–38, Feb. 2019.
- [20] F. Khateb, T. Kulej, M. Kumngern, W. Jaikla, and R. K. Ranjan, “Comparative performance study of multiple-input bulk-driven and multiple-input bulk-driven quasi-floating-gate DDCCs,” *AEU-Int. J. Electron. Commun.*, vol. 108, pp. 19–28, Aug. 2019.

- [21] M. Kumngern, F. Khateb, and T. Kulej, "Extremely low-voltage low-power differential difference current conveyor using multiple-input bulk-driven technique," *AEU-Int. J. Electron. Commun.*, vol. 123, Aug. 2020, Art. no. 153310.
- [22] M. Kumngern, F. Khateb, and T. Kulej, "0.3 V differential difference current conveyor using multiple-input bulk-driven technique," *Circuits, Syst., Signal Process.*, vol. 39, no. 6, pp. 3189–3205, Jun. 2020.
- [23] F. Khateb, M. Kumngern, T. Kulej, and C. Psychalinos, "0.5 V universal filter based on multiple-input FDDAs," *Circuits, Syst., Signal Process.*, vol. 38, no. 12, pp. 5896–5907, Dec. 2019.
- [24] M. Kumngern, N. Aupithak, F. Khateb, and T. Kulej, "0.5 V fifth-order butterworth low-pass filter using multiple-input OTA for ECG applications," *Sensors*, vol. 20, no. 24, p. 7343, Dec. 2020.
- [25] M. Kumngern, T. Kulej, F. Khateb, V. Stopjakova, and R. K. Ranjan, "Nanopower multiple-input DTMOs OTA and its applications to high-order filters for biomedical systems," *AEU-Int. J. Electron. Commun.*, vol. 130, Feb. 2021, Art. no. 153576.
- [26] M. Kumngern, T. Kulej, V. Stopjakova, and F. Khateb, "0.5 V sixth-order chebyshev band-pass filter based on multiple-input bulk-driven OTA," *AEU-Int. J. Electron. Commun.*, vol. 111, Nov. 2019, Art. no. 152930.
- [27] W. Jaikla, F. Khateb, M. Kumngern, T. Kulej, R. K. Ranjan, and P. Suwanjan, "0.5 V fully differential universal filter based on multiple input OTAs," *IEEE Access*, vol. 8, pp. 187832–187839, 2020.
- [28] C. A. De La Cruz-Blas, M. P. Garde, and A. Lopez-Martin, "Super class AB transconductor with slew-rate enhancement using QFG MOS techniques," in *Proc. Eur. Conf. Circuit Theory Design (ECCTD)*, Catania, Italy, Sep. 2017, pp. 1–4, doi: [10.1109/ECCTD.2017.8093308](https://doi.org/10.1109/ECCTD.2017.8093308).
- [29] T. Tsukutani, M. Higashimura, N. Takahashi, Y. Sumi, and Y. Fukui, "Versatile voltage-mode active-only biquad with lossless and lossy integrator loop," *Int. J. Electron.*, vol. 88, no. 10, pp. 1093–1101, Oct. 2001.
- [30] Texas Instruments. (2015). *LM13700: Dual Operational Transconductance Amplifier With Linearizing Diodes and Buffers*. [Online]. Available: <http://www.ti.com/product/LM13700>



**MONTREE KUMNGERN** received the B.S.Ind.Ed. degree from the King Mongkut's University of Technology Thonburi, Thailand, in 1998, and the M.Eng. and D.Eng. degrees from the King Mongkut's Institute of Technology Ladkrabang, Thailand, in 2002 and 2006, respectively, all in electrical engineering. In 2007, he has served as a Lecturer for the Department of Telecommunications Engineering, Faculty of Engineering, King Mongkut's Institute of Technology Ladkrabang.

From 2010 to 2017, he has also served as an Assistant Professor. He is currently an Associate Professor. He has authored or coauthored over 200 publications in journals and proceedings of international conferences. His research interests include analog and digital integrated circuits, discrete-time analog filters, non-linear circuits, data converters, and ultra-low voltage building blocks for biomedical applications.



**FABIAN KHATEB** received the M.Sc. and Ph.D. degrees in electrical engineering and communication and the M.Sc. and Ph.D. degrees in business and management from the Brno University of Technology, Czech Republic, in 2002, 2003, 2005, and 2007, respectively. He is currently a Professor with the Department of Microelectronics, Faculty of Electrical Engineering and Communication, Brno University of Technology, and the Department of Information and Communication Technology in Medicine, Faculty of Biomedical Engineering, Czech Technical University in Prague. He holds five patents. He has authored or

coauthored over 100 publications in journals and proceedings of international conferences. He has expertise in new principles of designing low-voltage low-power analog circuits, particularly biomedical applications. He is also a member of the Editorial Board of *Microelectronics Journal*, *Sensors*, *Electronics*, and *Journal of Low Power Electronics and Applications*. He is also an Associate Editor of *IEEE Access*, *Circuits, Systems and Signal Processing*, *IET Circuits, Devices & Systems*, and *International Journal of Electronics*. He was a Lead Guest Editor for the special issues on Low Voltage Integrated Circuits and Systems on Circuits, Systems and Signal Processing in 2017, *IET Circuits Devices & Systems* in 2018, and *Microelectronics Journal* in 2019. He was also a Guest Editor for the special issue on Current-Mode Circuits and Systems; Recent Advances, Design and Applications on *International Journal of Electronics and Communications* in 2017.



**TOMASZ KULEJ** received the M.Sc. and Ph.D. degrees (Hons.) from the Gdańsk University of Technology, Gdańsk, Poland, in 1990 and 1996, respectively. He was a Senior Design Analysis Engineer with polish branch of Chipworks Inc., Ottawa, ON, Canada. He is currently an Associate Professor with the Department of Electrical Engineering, Częstochowa University of Technology, Poland, where he conducts lectures on electronics fundamentals, analog circuits, and computer aided

design. He has authored or coauthored over 80 publications in peer-reviewed journals and conferences. He holds three patents. His research interests include analog integrated circuits in CMOS technology, with emphasis to low voltage and low power solutions. He also serves as an Associate Editor for the *Circuits Systems and Signal Processing* and *IET Circuits Devices and Systems*. He was also a Guest Editor of the special issues on Low Voltage Integrated Circuits on Circuits Systems and Signal Processing in 2017, *IET Circuits Devices and Systems* in 2018, and *Microelectronics Journal* in 2019.



**COSTAS PSYCHALINOS** (Senior Member, IEEE) received the B.Sc. and Ph.D. degrees in physics and electronics from the University of Patras, Greece, in 1986 and 1991, respectively.

From 1993 to 1995, he worked as a Postdoctoral Researcher with the VLSI Design Laboratory, University of Patras. From 1996 to 2000, he was an Adjunct Lecturer with the Department of Computer Engineering and Informatics, University of Patras, Greece. From 2000 to 2004, he has served as an Assistant Professor for the Electronics Laboratory, Department of Physics, Aristotle University of Thessaloniki, Greece. Since 2004, he has been serving as a Faculty Member for the Electronics Laboratory, Department of Physics, University of Patras, where he is currently a Full Professor. His research interests include the continuous and discrete-time analog filtering, including fractional-order filters, companding filters, current amplifier filters, CCII and CFOA filters, and sampled-data filters, and in the development of ultra-low voltage building blocks for biomedical applications. He is also a member of Nonlinear Circuits and Systems Technical Committee of the IEEE CAS Society. He also serves as an Area Editor for the *International Journal of Electronics and Communications (AEU)* journal, and an Editor for the *International Journal of Circuit Theory and Applications*. He is also an Associate Editor of the *Circuits Systems and Signal Processing Journal* and the *Journal of Advanced Research*. He is also a member of the Editorial Board of the *Analog Integrated Circuits and Signal Processing Journal*, *Microelectronics Journal*, and *Journal of Low Power Electronics*.